Journal of Thermal Analysis and Calorimetry
https://doi.org/10.1007/s10973-022-11285-9

Solid wood impregnated with a bio-based phase change material for low temperature energy storage in building application

Meysam Nazari[1] · Mohamed Jebrane[1] · Nasko Terziev[1]

Received: 24 August 2021 / Accepted: 17 February 2022
© The Author(s) 2022

Abstract

Wood impregnated with a multicomponent mixture of fatty acids as a bio-based phase change material (BPCM) to improve its thermal characteristics was studied. The studied wood/BPCM composites can be used as internal elements in buildings for energy storage. Scots pine and beech sapwood were impregnated with a multicomponent mixture of linoleic acid and coconut oil fatty acids at a ratio of 20:80. Leakage test was conducted and revealed that the maximum leakage for pine and beech were 9 and 8%, respectively. Light microscopy was employed to demonstrate the distribution of the BPCM in the wood structure. Rays in both pine and beech wood served as pathways for impregnation of the BPCM to partly fill the tracheid lumens (pine) and vessels (beech). Thermal characterization of the studied samples employed T-history and DSC methods, concluding that the impregnated wood had significant thermal mass, ability to store excessive energy in terms of latent heat and keep the temperature constant for long time. The specific heat capacity of the impregnated samples was 4–5 J g^{-1} K^{-1} i.e., higher than that of the untreated control samples of ca. 2 J g^{-1} K^{-1}. The thermal conductivity of the samples before and after the impregnation was measured using heat flow meter method and the results showed that the untreated beech wood had higher thermal conductivity compared to pine and the parameter improved when the cell lumens were filled with the BPCM. Scots pine wood with to 80% mass percentage gain (MPG) after impregnation demonstrated an increment in thermal conductivity of 33% while Scots pine and beech with 43 and 38% MPG demonstrated an increase of the conductivity with 8 and 11%, respectively.

Keywords Beech · Bio-based PCMs · Building applications · Energy storage · Impregnation · Leaching · PCM distribution · Scots pine · Thermal characterization

Abbreviations

BPCM	Bio-based phase change materials
CoFA	Coconut oil fatty acid
DSC	Differential scanning calorimetry
LA	Linoleic acid
PCM	Phase change materials

List of symbols

A	Heat transfer area [m^2]
C_p	Specific heat [J g^{-1} K^{-1}]
L	Thickness of the samples [m]
m	Mass of the samples [kg]
P	Independent variables
Q	Heat [W]
q/a	Heat flux [W m^{-2}]
R	Dependent variables
T	Temperature [ºC]
t	Time [s]
U	Uncertainty
u	Overall heat transfer coefficient [W m^{-2} K^{-1}]

Greek symbol

λ	Thermal conductivity [W m^{-1} K^{-1}]
Δ	Difference
∞	Ambient

Subscripts

f	Final
i	Initial
n	Time point
ref	Reference
$samp$	Sample

✉ Mohamed Jebrane
mohamed.jebrane@slu.se

[1] Department of Forest Biomaterials and Technology, Swedish University of Agricultural Sciences, Vallvägen 9C, 750 07 Uppsala, Sweden

Published online: 16 March 2022

Introduction

Development of bio-materials from renewable sources is essential for future technologies to harmonize the human living environment [1]. The building industry has an overall positive outlook and guarantees future interest in bio-based products, with high percent of using timber in single and multi-floor buildings during the last decade [2, 3].

Traditionally used construction materials including metals, concrete, insulation polymers and plastics impose environmental problems, e.g. non-recyclable wastes. Globally, around half of the construction materials origins from non-renewable resources. Moreover, the embodied energy of building material is responsible for 10–20% of the building's total energy consumption. In addition, some materials (asbestos, formaldehyde, and lead) can have a harmful effect on the human's health. A sustainable solution can be the increased utilisation of renewable bio resource construction materials for a better indoor environment and reduction of the negative impacts on climate and health [4]. Considering the above, the demand for environmentally friendly, renewable and green building materials has increased significantly over the past few years and it is expected to grow continuously[5]. Green building materials used in constructions to energy management have a crucial relevance to achievement of sustainable development goals (SDGs). A study [6] showed that SDGs 7.3, 11.6 and 13.2 are essentially achievable by increased building with bio-materials. In order to address the mentioned problems related to non-renewable construction materials, more attention lays on engineered wood elements as bio-based, renewable, sustainable and recyclable material to replace currently used traditional materials in modern single and multistory building constructions [5]. Manufacturing of wooden-based construction materials demands less energy compared to steel and concrete and the wastes are recycable [7].

Low thermal mass of wood limits its energy efficiency when it is used for internal applications. The wood material cannot store and release extra energy in case of temperature fluctuation and thus, extra energy should be supplied to compensate and regulate the energy balance inside buildings. This issue might be even more apparent for cold climate regions where a large amount of the generated energy is expended for heating during winter. However, if wooden panels are engineered in a combination with bio-based phase change materials, e.g. fatty acids or esters with appropriate working temperature, the temperature fluctuation inside buildings can be controlled. Stored latent heat can be released when the temperature drops down under the comfort temperature and the energy is applied more efficiently [8–10]. The progress in the design of new timber systems, e.g. konstruktionsvollholz (KVH), duo/trio laminated beams, cross-laminated timber (CLT) and laminated veneer lumber (LVL) offers new options for the integration of bio-based phase change materials (BPCM) to increase the efficiency and reduce the energy demand of the buildings.

Wood in various forms (fibers, flour, solid wood, veneer) is a cheap bio-container for encapsulation of PCMs, widely used as a building material and thus, can naturally be integrated with BPCMs [9]. BPCMs can be incorporated in the internal walls or in its coatings [11], flooring [10] or in the façades of the buildings [12]. As energy savings become an inevitable part of modern buildings, synergy between BPCM and wood comprises various options, e.g. wood flour [13, 14], and surface treatment of solid wood and wood composites [15–17] to host the BPCMs.

The majority of studies concentrated on wood/PCM composites where the wood can be in a form of flour, solid or delignified wood. Examples are fatty acids or their mixtures were impregnated in wood flour [18, 19] for increased latent heat storage in the composites. Paraffin was blended with poplar wood flour [20] in a bio-composite with latent heat capacity of 26.8 J g^{-1} while graphite was added to improve the thermal conductivity of the material.

Recently, delignified wood has been studied intensively, e.g. an eutectic mixture of capric-palmitic acids impregnated into delignified wood [21] at a retention of 61.2% demonstrated no leakage, a phase transition temperature of 23.4 °C and latent heat of 94.4 J g^{-1} with good thermal stability. Another study [22] used delignified wood as an encapsulating material for impregnation of PCM claiming increased pore volume compared to the initial material. However, the approach of using delignified wood is debatable since lignin, having best thermal conductivity of the three structural polymers in wood, has been extracted.

Solid wood of alder [23] impregnated with paraffin and coated with polystyrene to avoid the leakage of the PCMs. An optimum mass percentage gain of 29.9 mass% and a latent heat value of 20.62 J g^{-1} was reported. Temiz et al. [24] studied Scots pine sapwood impregnated with an eutectic mixture of capric acid (CA) and stearic acid (SA). After thermal characterization of the material, it was concluded that the system wood/CA-SA can be used for indoor temperature regulation and energy saving in timber buildings. Solid wood as a BPCM carrier is particularly suitable for flooring. Because of the floor heating systems construction, the engineered wood floor can undergo many heating/cooling phases and thus, ensure significant gain of latent heat. In a study, Mathis et al. [10] engineered the thin upper layer of wood flooring for absorbing and storing solar energy at a temperature of 30 °C. Oak and sugar maple wood impregnated with a commercial microencapsulated BPCM (Nextek29) was studied and a latent heat of 7.6 J g^{-1} for the composite

with 77% improvement in thermal mass compared to the untreated wood was found.

The research ideas above still have to cope with the inherited disadvantages of wood namely, moderate heat capacity and low thermal mass and thus, low ability to absorb and store thermal energy, low thermal conductivity, dimensional instability and bio-degradability.

The approach of using wood/BPCM composites for passive energy storage within the comfort temperature range should address certain questions including comprehensive studies regarding the impregnability, leaching of the BPCM, and comprehensive thermal analyses of the composite including temperature behavior, thermal mass, heat capacity, thermal conductivity and enthalpy. The material characterisation must be carried out in a comparison with untreated wood and/or other building materials. Wood impregnability and leaching of the BPCM have often been neglected and there is a scarcity of information about the impregnation of BPCMs in the wood cell wall and lumen. According to the current knowledge, the above questions have rarely been studied comprehensively to show deeper interaction between BPCM and the wood matrix. A drawback of previous studies is the use of small size samples for DSC, which cannot give deep understanding and insight of the thermal behavior of the entire composite.

The present study focuses on solid wood of two widely used wood species for building in Europe namely, Scots pine (softwood) and beech (hardwood). A special emphasis has been set on the impregnability of the wood and a study on leaching was conducted to analyze the problem when a recently developed BPCM [25] has been selected and employed. The aim of the study was to reveal the thermal characteristics of the solid wood using DSC, T-history and heat flow meter method to investigate the feasibility of the two wood species for encapsulation of the BPCM for building purposes.

Experimental

Materials

A previously developed BPCM composed of coconut oil fatty acids (CoFA) and linoleic acid (LA) mixed in a ratio of 80:20 [25] was used through the study. Polyethylene glycol with an average molecular mass of 600 (PEG 600) was purchased from Sigma-Aldrich and was used as a reference PCM in the leaching test. Wood samples of Scots pine (*Pinus sylvestris* L.) sapwood and beech (*Fagus sylvatica* L.) with dimensions of 9 × 90 × 90 mm along the grain and without visible defects were used throughout the study.

Methods

Incorporation of PCMs into wood and leaching test

The BPCM was impregnated in the wood samples by a vacuum-pressure process in an autoclave. Target retentions expressed by the mass percentage gain (MPG) of the sample were set to 55 and 90%, i.e. low and high. The autoclave temperature was set to 60 °C to ensure melting of the BPCM. PEG 600 was impregnated only in Scots pine samples. The wood samples were conditioned in a climate chamber to 12% moisture content prior to the impregnation. The high MPG was achieved by immersing the samples in BPCM and applying a vacuum of 350 mbar for 10 min followed by 6 bar pressure for 1 h. The low MPG was achieved when a pre-pressure of 0.75 bars for 60 min was applied instead of vacuum step. Wood density, impregnation parameters and the average MPG are shown in Table 1.

The MPG was calculated as the difference between the initial (m_i) and final mass (m_f) of the wood sample and expressed in percent (Eq. 1).

Table 1 Wood density, impregnation parameters and average MPG. Standard deviations in parentheses, 5 samples per treatment

Wood species	Density, kg m^{-3}	PCM	Time and vacuum depth	Pre-pressure time	Pressure time	Average MPG, %
Scots pine	506/88	PEG 600	–	60 min 0.75 bar	–	Low 59.8/1.9
		PEG 600	10 min 80%	–	60 min 6 bar	High 88.3/2.5
		BPCM	–	60 min 0.75 bar	–	Low 56.3/3.7
		BPCM	10 min 80%	–	60 min 6 bar	High 94.7/5.7
Beech	745/53	BPCM	10 min 80%	–	60 min 6 bar	43.1/4.4

$$\text{MPG}\ (\%) = \frac{\left(m_f - m_i\right)}{m_i} \times 100 \quad (1)$$

After the impregnation, the samples were conditioned in a cold room (10 °C) for 3 weeks and the mass was recorded prior to the leaching tests. To assess the leaching rate, each impregnated sample was placed between spruce and oak samples. Both spruce and oak samples had identical dimensions as the treated sample and were conditioned at room climate prior to the test. The 3-layer set was pressed by a mass of 1 kg and placed in a climate chamber at 35 °C for 24 h. The cumulative leached amount of BPCM was calculated as a difference between the mass of the sample after 8, 16 and 24 h and related to the initial mass and expressed in percent (likewise Eq. 1).

Light microscopy

Impregnated and leached samples were cut to sub-samples; only those located in the inner part of the samples were taken for microscopy observations. The sub-samples had dimensions of 5 × 5 × 15 mm and semi-thin Sections (20–40 µm) were cut by a Leitz sliding microtome (Leitz, Wetzlar, Germany) and examined using Leica DMLB light microscope (Leica, Wetzlar, Germany). No additional treatments to soften the wood before cutting were applied.

Osmium tetroxide (OsO_4) was used as a specific/chemical marker known to react strongly with ethylene bonds of unsaturated triglycerides being reduced to osmium black (OsO_2). Apart from its common use as a post-fixative for electron microscopy, it reacts strongly with the ethylene bonds of a number of fatty acids including the cis-linoleic acid and cis-linolenic acids [26] used here in the present BPCM preparation.

To visualize the BPCM in the wood structure, observations were made on sections from the inner regions of the samples treated with 1% w/v of OsO_4 for 1 h at room temperature. Some wood sections were stained with Oil Red O that reacts and stains also the available fatty acids. The untreated Scots pine and beech sections were stained with safranin.

Differential scanning calorimetry (DSC)

Differential scanning calorimetry (DSC) curves of the PCM and PCM impregnated into wood were recorded on a DSC Mettler-Toledo DSC 3 system under a nitrogen atmosphere. For each DSC run, a sample of mass usually in the range 14–20 mg was taken from the core of each sample and hermetically sealed in a standard DSC aluminum crucible pan. The DSC tests were conducted between − 25 and 50 °C at a heating rate of 2 °C min^{-1} with 15 min isothermal segment at each − 25 and 50 °C. This heating–cooling cycle was repeated three times to obtain an acceptable reproducibility. Prior to measurements, the DSC system was calibrated using indium and zinc.

Thermal conductivity of PCMs by heat flow meter method

Thermal conductivity of the wood/BPCM composite was measured according to the standard methods ASTM C1155-95 (2013) and ISO 9869-1:2014, known as heat flow meter method with some modifications [27, 28]. A schematic illustration of the experimental set-up used to measure the thermal conductivity is shown in Fig. 1. Since the purpose is to measure thermal conductivity along the thickness of samples, an insulated box was designed to minimize the heat loss from other sample's sides. Moreover, the samples are ten times bigger in other directions than thickness, which guarantees low heat loss from other directions. Two thermocouples of K- and T-type were used to measure the temperature at the both surfaces of the sample. To avoid the effect of the surrounding environment on the measurements, the non-contact surface of the thermocouples were insulated. A heat flux meter type FHF03 supplied from Hukseflux, the Netherlands was used to measure the heat flux at the surface exposed to cold environment. Each measurement was run for

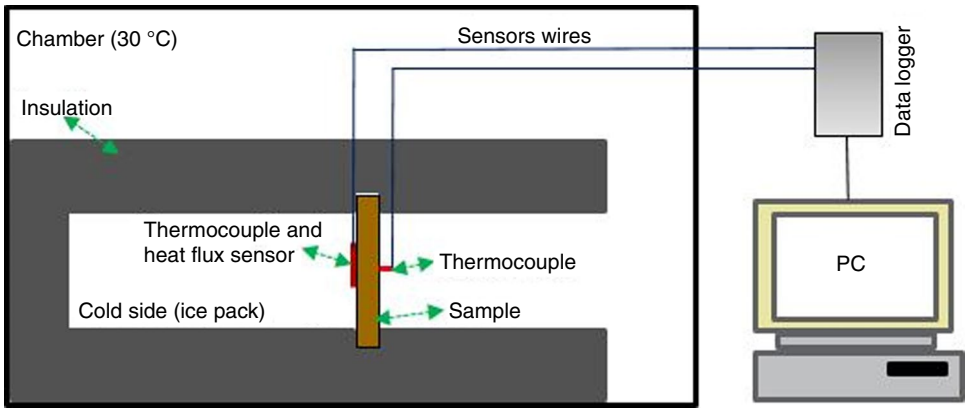

Fig. 1 Schematic diagram of the designed rig for thermal conductivity measurements

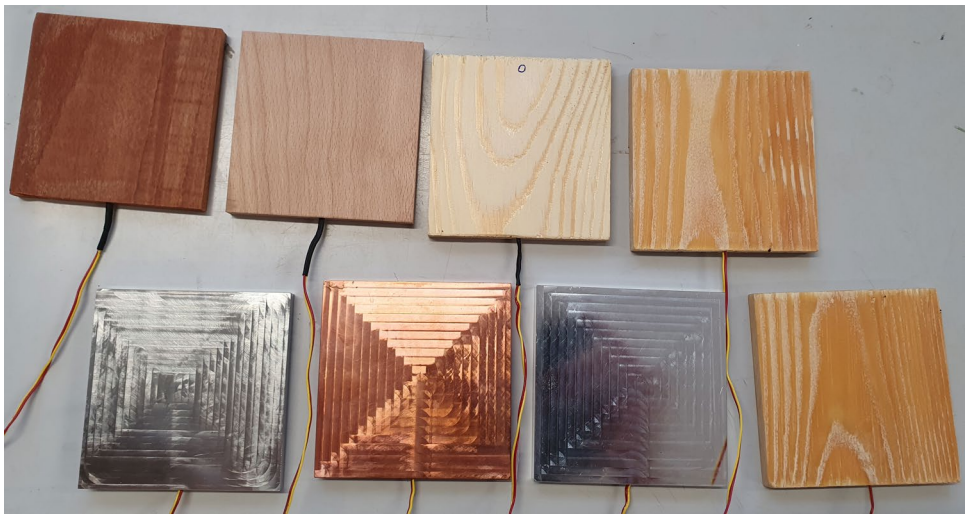

Fig. 2 Samples and references without insulation

Table 2 Thermal and physical properties of references

	Copper (SS 5011-04)	Aluminium (SS 4212)	Stainless steel (SS 2343)
Mass/g	657.6	200.3	581.9
Dimension/mm	9×90×90	9×90×90	9×90×90
Thermal conductivity/W m^{-1} K^{-1}	395	167–216	72–79
Specific heat capacity/J g^{-1} K^{-1}	0.385	0.89	0.45–0.46

3 h to ensure a steady state process [29] and the experiment was repeated 4 times for reproducibility. After measuring the heat flux and the temperatures at both surfaces of the samples, the thermal conductivity was calculated by applying Fourier's law of thermal conduction [29]:

$$\lambda = \frac{q}{a} \times \frac{\Delta L}{\Delta T}, \tag{2}$$

where $\frac{q}{a}$ is the heat flux, ΔL is the thickness, and ΔT is temperature difference.

T-history, specific heat capacity and enthalpy

T-history method was used to measure thermal properties of several samples simultaneously [30, 31] including melting/freezing point, latent heat of fusion, degree of super cooling and specific heat capacity. Untreated control wood samples, samples impregnated with BPCM (wood/BPCM composites), and metal plates (copper, aluminum and stainless steel) with identical dimensions were tested simultaneously (Fig. 2). The copper plate was used as main reference to obtain overall heat transfer coefficient (u). This parameter was then used to calculate the thermal properties of aluminum and stainless steel, which were then compared with the known data of these materials (Table 2) to verify and validate our approach. The samples and references were

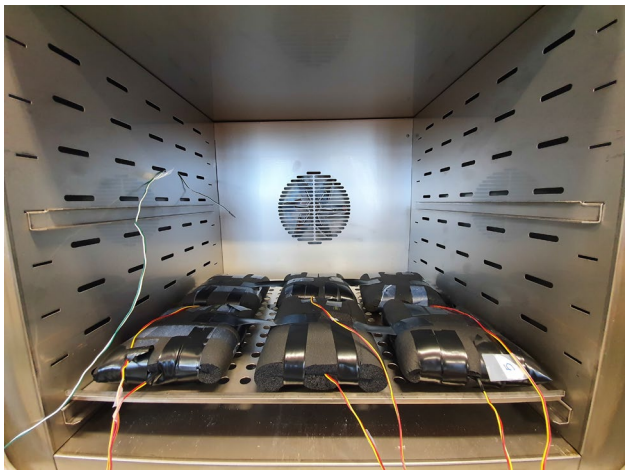

Fig. 3 Insulated samples and references inside the chamber

thermally insulated using 10 mm thickness ARMAFLEX insulation material (Fig. 3). K-type thermocouples were used to record temperature changes over time for samples and references. The thermocouples were placed at the centerline and in the middle of the samples. For cold and hot ambient climates, two chambers were employed, the former used for cold ambient climate fixed at 10 °C, while the latter chamber was used for hot ambient climate set at 35 °C. The

chamber's temperatures were recorded with two separate thermocouples. Figures 2 and 3 show the photographs of the samples and references with and without insulation. Thermal and physical properties of the references are summarized in Table 2. Samples and references were first preheated at 35 °C, and then quickly transferred into the chamber at 10 °C and the temperature profile was recorded. Once the equilibrium temperature was reached (ca. 3 h), the samples and the references were transferred back at 35 °C and the temperature changes were recorded.

Energy balance for the reference was employed to obtain the overall heat transfer coefficient. Since the wooden samples and the metal reference have identical dimensions and insulation for uniform heat transfer conditions, the overall heat transfer coefficient (u) for both reference and wood samples were considered identical. The amount of heat transferred to/from samples in the chamber is expressed as follow:

$$Q = uA\left(T(t)_{\mathrm{n}} - T_{\infty}\right), \tag{3}$$

where Q, u, A, $T(t)_{\mathrm{n}}$ and T_{∞} are, respectively, the transferred heat, overall heat transfer coefficient, heat transfer area, sample temperature at each time point and ambient temperature inside oven/chamber.

The amount of heat stored/released from samples is:

$$Q = mC_{\mathrm{p}}\frac{\mathrm{d}\left(T_{\mathrm{i}} - T(t)_{\mathrm{n}}\right)}{dt}, \tag{4}$$

where m, C_{p}, T_{i} and dt are, respectively, the mass of the samples, specific heat capacity, initial temperature and time interval.

The amount of transferred energy to/from the samples is stored/released in/from the samples, then the energy balance is:

$$Q = -uA\left(T(t)_{\mathrm{n}} - T_{\infty}\right) = mC_{\mathrm{p}}\frac{\mathrm{d}\left(T(t)_{\mathrm{n}} - T_{\mathrm{i}}\right)}{dt} \tag{5}$$

By rearrangement and integration, the temperature distribution for the reference and wood samples are obtained as:

$$\int_{T_{\mathrm{i}}}^{T_{\mathrm{n}}} \frac{d\left(T(t)_{\mathrm{n}} - T_{\infty}\right)}{\left(T(t)_{\mathrm{n}} - T_{\infty}\right)} = -\int_{0}^{t_{\mathrm{n}}} \frac{uA}{mC_{\mathrm{p}}}dt \tag{6}$$

After mathematical operation:

$$\ln\left[\frac{\left(T(t)_{\mathrm{n}} - T_{\infty}\right)}{\left(T_{\mathrm{i}} - T_{\infty}\right)}\right] = -\frac{uA}{mC_{\mathrm{p}}}t_{\mathrm{n}} \tag{7}$$

As the thermo-physical properties of the reference is known, the overall heat transfer coefficient (u) is calculated using energy balance for the reference:

$$uA = -\frac{\ln\left[\frac{\left(T(t)_{\mathrm{n}} - T_{\infty}\right)}{\left(T_{\mathrm{i}} - T_{\infty}\right)}\right]_{\mathrm{ref}}}{t_{\mathrm{n}}} m_{\mathrm{ref}}C_{\mathrm{p,ref}} \tag{8}$$

uA is calculated by the energy balance for the reference according to Eq. 8, and as heat transfer area and conditions around reference and wood samples are identical, uA was calculated from the energy balance of the reference and used further to calculate C_{p} for the wood samples. After substitution Eq. 8 in Eq. 7, C_{p} of the samples is calculated as:

$$C_{\mathrm{p,samp}} = \frac{\ln\left[\frac{\left(T(t)_{\mathrm{n}} - T_{\infty}\right)}{\left(T_{\mathrm{i}} - T_{\infty}\right)}\right]_{\mathrm{ref}}}{\ln\left[\frac{\left(T(t)_{\mathrm{n}} - T_{\infty}\right)}{\left(T_{\mathrm{i}} - T_{\infty}\right)}\right]_{\mathrm{samp}}} \frac{m_{\mathrm{ref}}}{m_{\mathrm{samp}}} C_{\mathrm{p,ref}} \tag{9}$$

Enthalpy of the samples is obtained as [25]:

$$\Delta H = c_{\mathrm{p,samp}}\left(T(t)_{\mathrm{n,\ samp}} - T_{\mathrm{samp,i}}\right), \tag{10}$$

where ΔH is enthalpy change from initial point to each time point n.

Results and discussion

Impregnation, leaching and PCM distribution

Under the studied conditions, MPG of up to 95% were achieved for pine, while a maximum of 43% MPG was possible for beech (Table 1). This is due mainly to the density and the anatomical features of beech. After impregnation and conditioning, the samples were leached at 35 °C and the cumulative rates of leached BPCM after 8, 16 and 24 h are plotted in Fig. 4.

Porous materials with low density, large internal surface area and various dimensions of cell lumens and cell wall cavities are suitable for storage of BPCMs. Nevertheless, most of the PCMs are susceptible to leakage [32] and thus, any lignocellulose material as a form of encapsulation can hardly prevent the leakage during exploitation [33]. Contrary, composite materials with additives, e.g. wood flour [34], wood-polymer composites [35] or copolymers [36] demonstrated no leaching. The above findings can be questioned since the leaching has been monitored after short time of 15–30 min. Compared to the mentioned encapsulation forms, the incorporated BPCM into solid wood in this study displayed low leaching rates under tested conditions. Due to the chemical structure and the molecular mass of PEG 600, this material leaches more than BPCM (*ca.* 7–8% PEG 600 vs. 2–4% PBCM). Regardless the initial retention, PEG 600 leaches gradually until it reaches *ca.* 12% after 24 h. The BPCM showed better stability in the wood and only a total of *ca.* 8 to 9% were leached for the low and

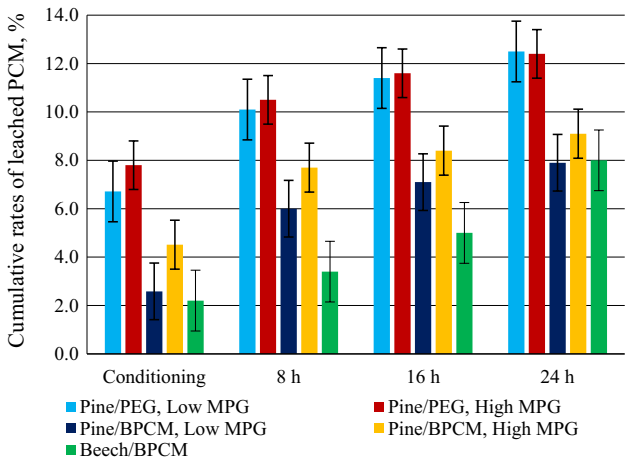

Fig. 4 Leaching rates of PEG 600 and BPCM from Scots pine and beech samples after 24 h at 35 °C. The real values of the target retentions of 50 and 90% are shown in Table 1

high MPGs. It should be mentioned that the effect of moisture is not considered in the results above. Particularly, in the stage of conditioning, some moisture will be adsorbed in the wood and thus, the actual value of leaching should be somewhat higher. The beech samples showed a similar leaching behavior as pine reaching 8% leachate after 24 h. Apparently, leaching is a serious hinder in the application of BPCMs since a significant part of the material can be lost. The demonstrated values are only after short period but the trend shows that the process will continue further and higher values will be reached before the BPCM achieves the point of equilibrium with the ambient conditions.

The impregnated samples were studied by light microscopy (Fig. 5) to reveal the penetration and distribution of the BPCM within the wood structure. All images were derived by light microscopy observations on sections from the inner regions of the impregnated samples. Outer regions showed similar but more intense reactions. Dry sectioning of samples was conducted to prevent any diffusion of the BPCM using pretreatment with polar/unpolar liquids and to reduce possible smearing during the sectioning process. As the wood has a high hardness and the sections were quite thick, it was possible to focus on cell layers beneath the section surface thereby confirming the specific presence of the BPCM in the wood structure. OsO_4 as a staining agent is known to react with compounds in both vapor and liquid phases, thus it is not known which phase were responsible for the strong reactions recorded. A multi-illustration of the BPCM distribution in the wood structure of Scots pine and beech is shown in Fig. 5.

Safranin-stained untreated control sections of Scots pine and beech showed the structure without the BPCM, i.e. empty anatomical elements. Strong reactions of both OsO_4 and Oil Red O with the BPCM were observed in the lumens of early- and latewood tracheids (Fig. 5b, c) and in the tips of axial tracheids (Fig. 5c) of Scots pine samples where the fatty acid mixture was found as precipitate. Some tracheids were completely filled while in some other the BPCM was found distributed on the internal cell wall. Light microscopy and staining observations confirmed the pathway for penetration of the BPCM into the wood was via the rays with a strong purple-black staining of the contents of the ray tracheids and parenchyma cells (Fig. 5b, c); ray tracheid bordered pits and axial tracheid bordered pits recognized (Fig. 5c). The staining reaction within the tracheid lumens and rays cells was very strong (i.e. reflecting the amount of BPCM present) but even the reaction with secondary cell wall layers was distinct in the transverse sections colored with Oil Red O (Fig. 5b) where a yellowing of the middle lamella and S2 walls was noted. The RLS sections stained with OsO4 (Fig. 5c), a darkish staining was achieved confirming the presence of some amount of BPCM in the cell walls.

The pathway for penetration of the BPCM into the beech wood was via the rays with a strong blackish staining of the contents (Fig. 5e, f). The vessel lumens are only partly filled with the BPCM (Fig. 5e) because part of the material has been leached. The majority of beech fibers were found filled with the BPCM while the BPCM in the vessels was found distributed on the cell wall surface (Fig. 5e, f).

The above observations and the staining reactions of the cell walls are suggestive that in addition to penetration of the wall that a thin film is produced along the exposed surfaces of the cell walls. Unlike most polar oxidizing agents, OsO_4 is able to penetrate both hydrophobic (i.e. high surface tension) and hydrophilic (low surface tension) lipids thus within the 1 h period the treated wood cell walls would had allowed penetration.

Thermal conductivity measurement with heat flow meter

Figure 6 shows the result of the heat flow meter method. It depicts the temperatures at both sample's surfaces and the measured heat flux. The monitored parameter profiles reached their steady state after almost 1 h, while the tests was conducted for approximately 3 h [29, 37], and the result at the steady part was used to calculate the thermal conductivity of the samples using Eq. 2. The experimental uncertainty due to measurement instrument including thermocouple, heat flux sensor and caliper on results calculated from Eq. 2 was determined and found to be 3.34%. The details of the calculations are given in the experimental uncertainty analysis section.

The measured thermal conductivities of wood and wood/BPCM composites are plotted in Fig. 7. The thermal conductivity of pine and beech were 0.12 and 0.23 W m^{-1} K^{-1},

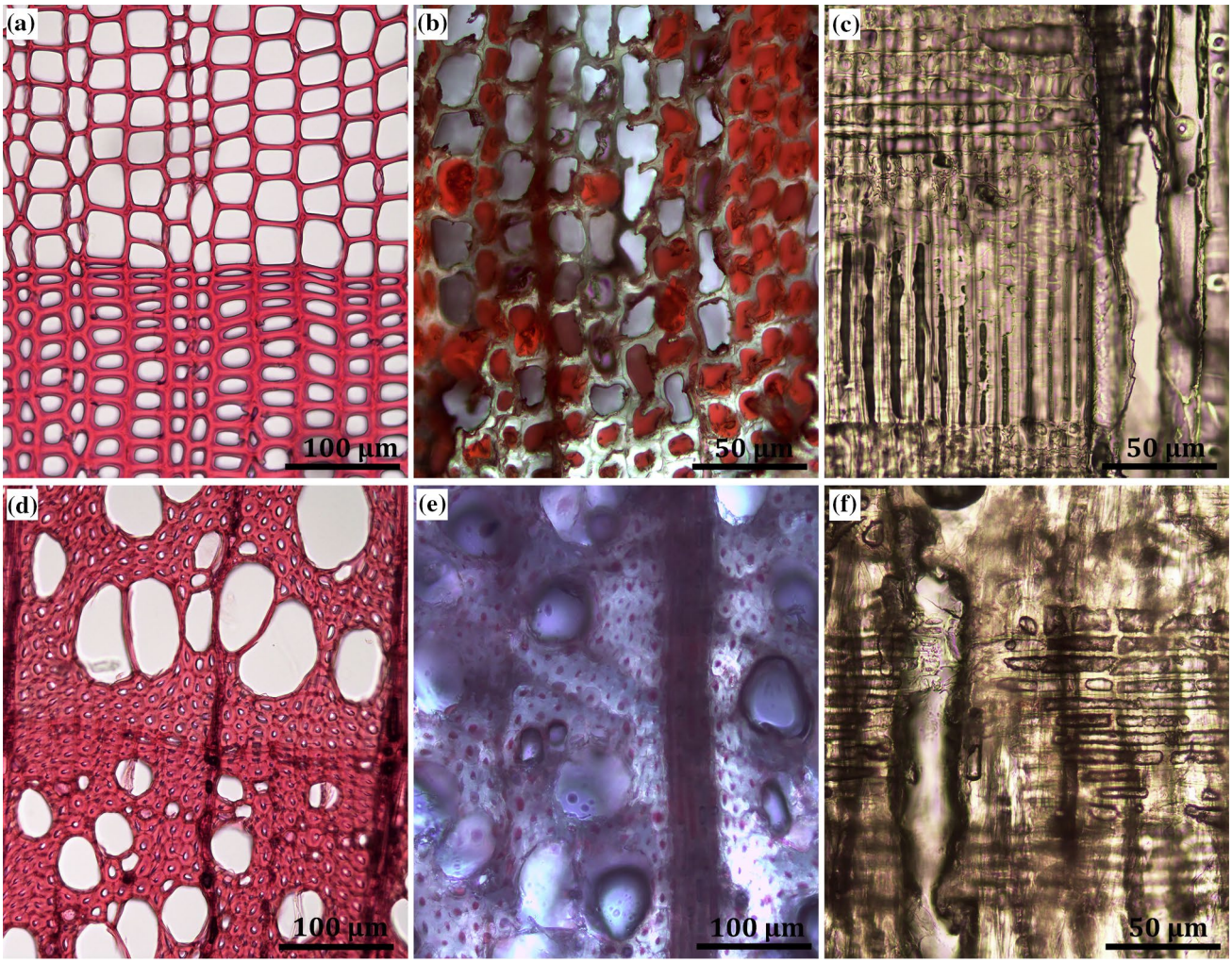

Fig. 5 Safranin (**a**, **d**), Oil Red O (**b**, **e**) and osmium tetroxide (**c**, **f**) staining of Scots pine and beech samples impregnated with BPCM. Scots pine (**a**, **b**), transverse sections (TS) of untreated wood (**a**) and precipitates of BPCM located in the cell lumens of tracheids (**b**) and at tracheid tips (**c**); Scots pine, radial-longitudinal section (RLS) section showing darkish staining of the BPCM present in the ray tracheids and parenchyma cells and in the bordered pits and latewood cell lumens (**c**). The entire wood structure has reacted and has a redish/blackish colouration. Beech (**d**, **e**), TS of untreated wood (**d**) and precipitates of BPCM located mainly in the fiber, rays and vessel lumens (**e**); Beech, TS and RLS of a broad homogeneous ray filled with BPCM (**e**, **f**). The adjacent vessel in (**f**) has a thin film of the BPCM on the cell wall surface

respectively, which were in line with the reported values in the literature [38, 39]. Previous studies [38] discussed that thermal conductivity of wood materials varies with density, moisture content and wood species. The thermal conductivity of pine was reported to be in the range 0.1–0.14 W m^{-1} K^{-1}, depending on the species. Czajkowski et al. [39] studied thermal conductivity of beech and reported a value of 0.24 W m^{-1} K^{-1} along the radial direction, while other study [38] reported a value of 0.19 W m^{-1} K^{-1}. These studies corroborate the funding of the present study.

The thermal conductivity of the BPCM was ca. 0.2 W m^{-1} K^{-1} at liquid state and ca. 0.35 W m^{-1} K^{-1} at solid state [25], i.e. higher than that of wood. The impregnated BPCM into wood is expected to improve the thermal conductivity of the composites. During thermal conductivity measurements, the temperature at the cold surface was 21–22 °C, while at the warm surface it was in the range 24–27 °C, indicating that the temperature of the composites was probably in the range 23–25 °C. This suggest that the BPCM inside the composites was at its mushy state during the tests. The thermal conductivity of BPCM at mushy state is slightly higher than liquid state; however, the exact value is unknown. The measured thermal conductivity of pine/BPCM composites with 43 and 78% MPGs were 0.13 and 0.16 W m^{-1} K^{-1}, respectively, which shows improvement of 8.3 and 33%, respectively. Beech/BPCM with 38% MPG, demonstrated a value of 0.255 W m^{-1} K^{-1}, showing 11% improvement.

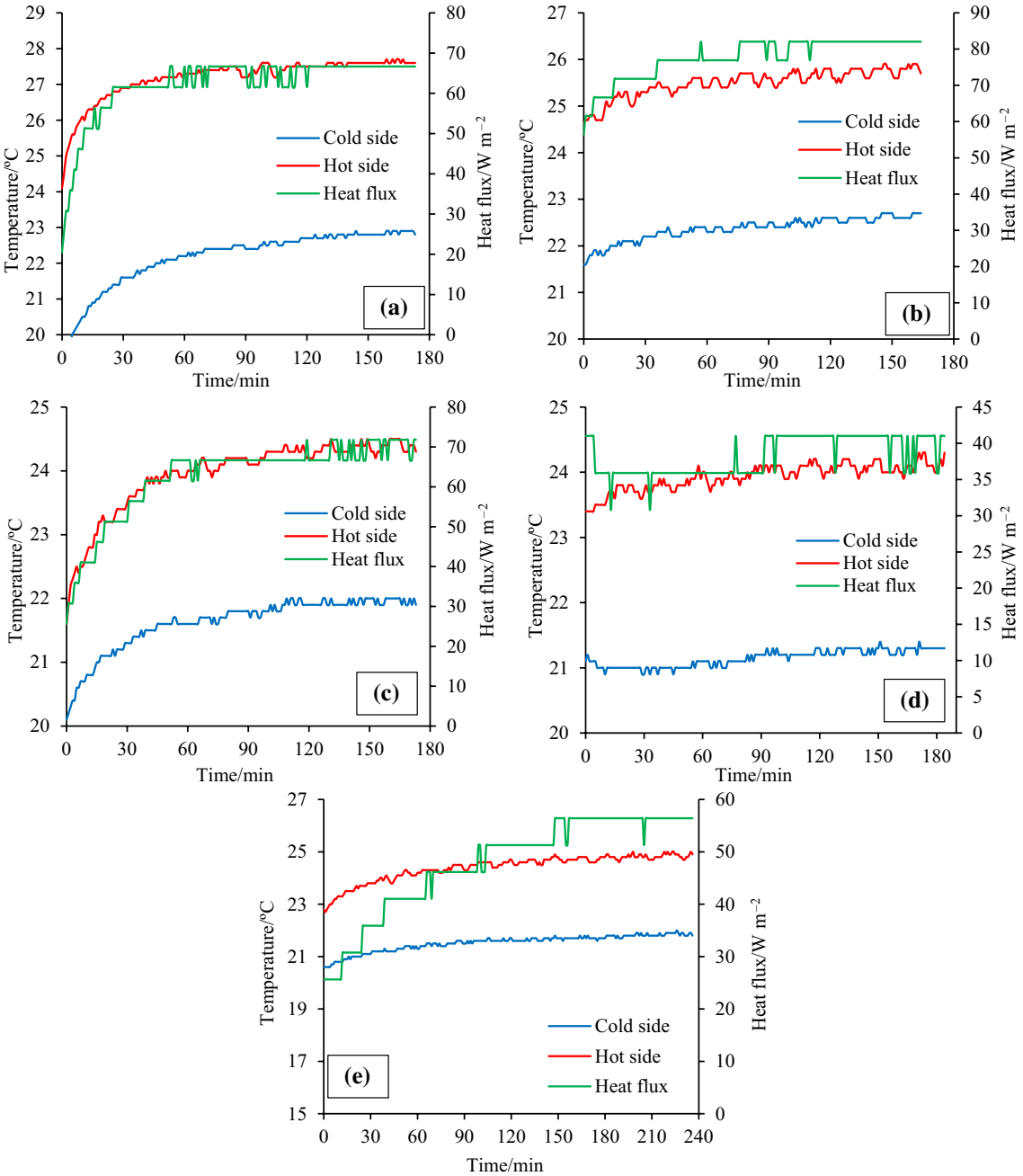

Fig. 6 Measured temperatures at both sides and heat flux for thermal conductivity. **a** Pine, **b** Beech, **c** Beech/BPCM 38%, **d** Pine/BPCM 43%, **e** Pine/BPCM 78%

The observed differences between impregnated pine and beech at comparable PCM retentions could be explained by the density and anatomical features of the wood species. The results showed also that the thermal conductivity increases with increasing of the MPG of BPCM. Yang et al. [40] studied the thermal properties of wood/PCM composite using carbonized pristine wood and 1-tetradecanol as PCM. The thermal conductivity value of the PCM at 25 °C was 0.241 W m^{-1} K^{-1}, for the carbonized wood at the same temperature and at radial direction, it was 0.414 W m^{-1} K^{-1}, while after full cell impregnation (maximum MPG), the thermal conductivity of the composite reached 0.515 W m^{-1} K^{-1}, thus showing 24% improvement. The study, likewise the present study showed that higher MPG leads to increase of the thermal conductivity.

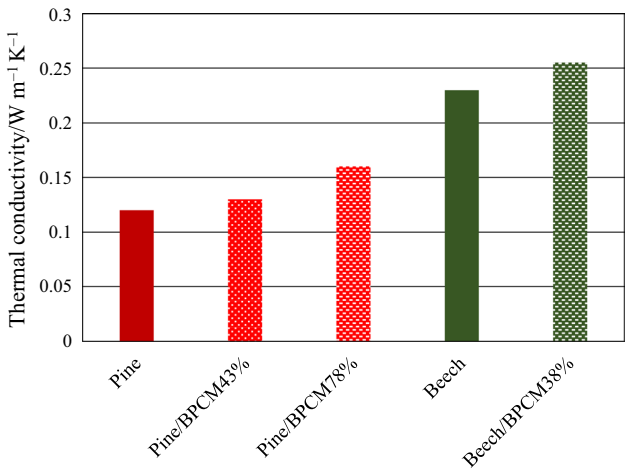

Fig. 7 Calculated thermal conductivity of the samples

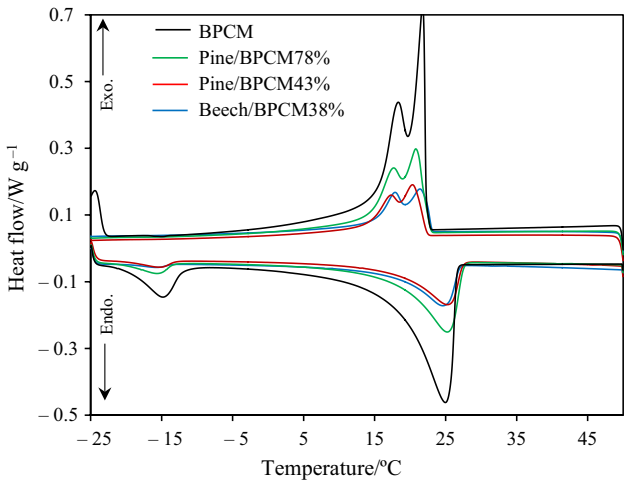

Fig. 8 DSC curves obtained for BPCM and for the wood/BPCM composites

Thermal analysis by DSC and T-history

Figure 8 shows the DSC curves obtained for BPCM (*80/20 ratio*) [25], and wood/BPCM composites. The patterns of heat flow for BPCM and Wood/BPCM composite were similar but with a slight shift in onset and endset temperatures. The heat flow and enthalpy measured for the wood/BPCM were lower than that of the pure BPCM, as the proportions of BPCM in the composite were ca. 43 and 78% for pine and 38% for beech, and the wood itself does not have latent heat. In addition, the most prominent peak of the pure BPCM decreased after incorporation in wood and two small peaks at lower temperatures, which are probably related to crystalline points of the BPCM were probably shifted to lower temperatures after impregnation into wood. The measured latent heat of fusion for BPCM was 94 J g^{-1} [25], but it was reduced to 30 and 43 J g^{-1} after incorporation into pine with 43 and 78% MPG and to 27 J g^{-1} for beech/BPCM with 38% MPG. Similar trend was reported [21, 40] when PCM was incorporated into wood. Yang et al. [40] studied carbonized wood fully impregnated with 1-tetradecanol as PCM, and reported a lower latent heat of fusion compared to pure PCM as a results of the reduction in latent heat per mass. By comparing carbonized and non-carbonized wood as supporting material, it was proven that the latent heat of the PCM/wood composite depends mainly on the content of PCM incorporated in the composite. Additional study [41] with delignified wood as substrate and a PCM retention of 65% reported lower latent heat of fusion than that of pure PCM. Ma et al. [21] used delignified and undelignified cedar wood as substrates impregnated with eutectic mixture of capric/palmitic acids at a retentions of 61.2 and 46.8%, respectively. A reduction in latent heat of fusion after incorporation into wood and a proportional relationship between the latent heat of fusion and the amount of impregnated PCM was reported. Additionally, a small temperature shift in onset and endset was reported.

Figure 9 shows the T-history profile for the samples and references during the cooling (9a) and heating process (9b). The copper plate (Cu) was used as the main reference and aluminum (Al) and stainless steel (SS) plates were used in order to validate the experimental results. The measured ambient temperatures were constant throughout the experiments with ± 0.8 °C maximum deviation. Once placed in the climate chamber at 10 °C, the samples and the references' temperatures decrease gradually from the starting temperature at 35 °C and continues to decease with the time until it reaches the chamber's ambient temperature (10 °C). During the course of cooling cycles, a phase change transition was observed for all the wood/BPCM composites at temperature around 22.3 °C which is lower than that of pure BPCM, which is around 24 °C. In addition, during cooling process the pure BPCM experienced a small degree of supercooling and solidifies incongruently, once impregnated into wood, no incongruence and supercooling were observed. During heating course, the pure BPCM and wood/BPCM composites melt congruently, and unlike the cooling course, the composites experiences a slight increase in phase transition temperature during heating cycle.

During the cooling and heating processes (Fig. 9), untreated pine and beech samples reached the equilibrium faster than the impregnated samples. For metal plates, Al reached the equilibrium quickly compared to Cu and SS due to the thermal mass (heat capacity, mC_p) of the samples. The temperature profile of the materials in transient conduction condition (Eq. 7) is a function of thermal mass of the materials (mC_p). Increment in (mC_p) leads to absorption and storage more energy by the material during heating and release more energy during cooling process, resulting in delay for

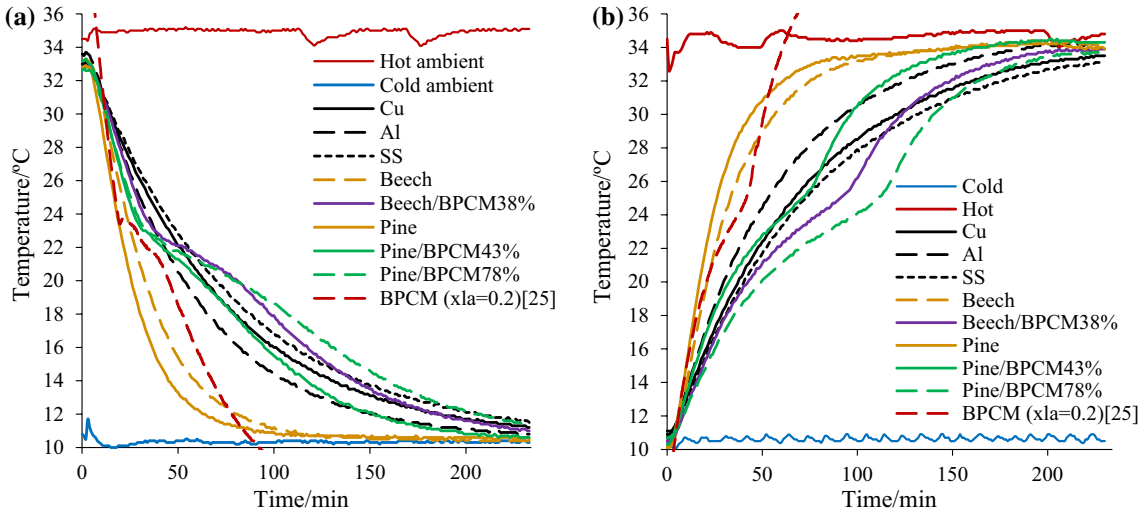

Fig. 9 T-history curves over cooling/heating cycle for **a** cooling and **b** heating

reaching the ambient temperature. Although pine and beech have comparable specific heat capacity, pine has less thermal mass than beech due to difference in density and thus, pine wood reached the ambient temperature faster. Despite high specific heat capacity of Al, its thermal mass was lower than that of Cu and SS, due to lower density.

Impregnation of BPCM into wood samples resulted in increase in thermal mass of the composite. Pine/BPCM at 43% MPG showed a thermal mass comparable to Al, and during the phase transition it performs as Cu and SS. For Beech/BPCM at 38% MPG, the thermal mass was found higher than pine composite with comparable retentions due to the higher thermal mass of beech. Beech/BPCM composite had even higher thermal mass than Cu and SS during the phase transition. Pine/BPCM at 78% MPG had highest mC_p and thus, able to absorb/release more energy.

Figure 10 shows the specific heat capacity for the tested samples calculated using Eq. 9 during cooling and heating processes. In this study, Cu was used as reference to calculate the overall heat transfer of the samples (Eq. 8), and then this parameter was used to calculate the specific heat capacity of other samples. Al and SS plates with known thermal characteristics were used to validate and approve the results. The measurements indicated that the specific heat capacity of Al and SS were 0.9 and 0.46 J g^{-1} K^{-1}, respectively, and were in line with the known properties of these materials (Table 2). As mentioned above, the heat capacity of wood is mainly temperature and moisture content dependent, while density and wood species has negligible effect

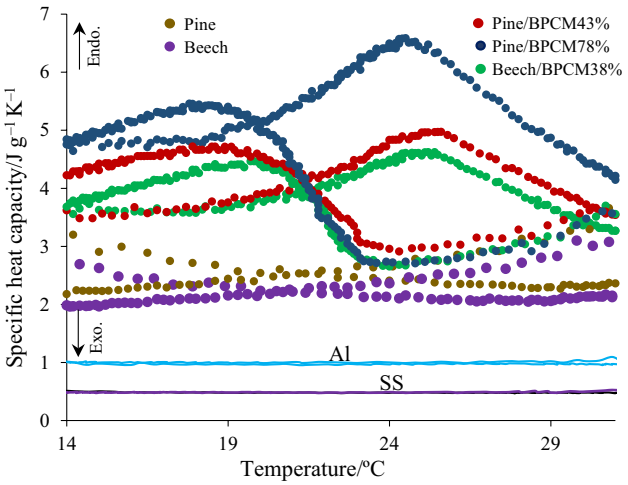

Fig. 10 Melting and freezing specific heat capacity for wood, composite samples, Al and SS

[38]. The measured heat capacity of wood at room temperature and moisture content of 12% was reported to be around 1.5–2 J g^{-1} K^{-1} [38]. In this study, the measured heat capacity of the untreated pine and beech samples were found to be ca. 2 J g^{-1} K^{-1}, similar to the reported results in the literature [38]. The results revealed that the incorporation of PCM into wood resulted in considerable improvement in specific heat capacity of the composite; the specific heat capacity increases proportionally to the content of the BPCM. The calculated heat capacity of beech/BPCM (38% MPG), pine/

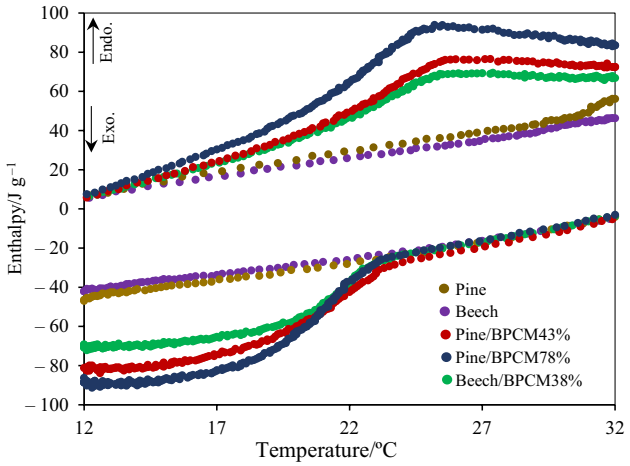

Fig. 11 Melting and freezing enthalpy for the samples

BPCM (43% MPG) and pine/BPCM (78% MPG) was ca. 3.8, 4.3 and 5 J g^{-1} K^{-1}, respectively.

Figure 11 shows the measured enthalpy for wood species and wood/BPCM composites during cooling and heating process. Untreated wood has no latent heat of fusion and the energy is stored as sensible heat during the heating, illustrated by a linear increase of enthalpy with temperature. Similar pattern was reported [10] where a dynamic heat flowmeter apparatus (DHFMA) was used to analyze heat storage capacity of wooden samples and it was found that during cooling, the untreated wood released the absorbed energy in a form of sensible heat identically to heating. The values obtained during cooling were negative indicating dissipation of energy to the ambient environment, while during heating the values were positive i.e., wood absorbed energy.

The wood/BPCM composites absorb and store heat in the form of latent heat during phase transition and in the form of sensible heat outside the transition region. The latent heat of pure BPCM is around 100 J g^{-1} [25], and it reduces to ca. 44 J g^{-1} for pine/BPCM composite of 78% MPG, and 30 J g^{-1} at 43% MPG, while this value for beech/BPCM at 38% MPG was ca. 30 J g^{-1}. The enthalpy values during cooling and heating process were found to be similar. The enthalpy of wood/PCM composite depends on the enthalpy of the PCM, whereby PCMs with higher enthalpy results in composite with additional enthalpy.

Thermal properties of tested samples with DSC, T-history and heat flow meter are tabulated in Table 3. Except some differences observed during the cooling, the results from DSC and T-history are in good agreement. T-history method used large samples that cooled down naturally in the chamber and thus, the results are more reliable [25] compared to the DSC where a limited amount of the sample was analyzed and the cooling rate affected the results.

Experimental uncertainty analysis

Experimental uncertainty associated with the thermal conductivity measurements by heat flow meter, specific heat capacity and enthalpy by T-history are introduced by the combination of the experimental errors, the calculations error and the accuracy of the measurement tools. In the current study, the overall errors were related to heat flux sensors, thermocouples, balance to measure mass of the samples, and the caliper to measure the dimensions of the samples. The uncertainty of the thermocouple is ± 0.1 °C, heat flux meter ± 0.001 W m^{-2}, balance and caliper are, respectively, 0.0000002 kg, and 0.00002 m. The uncertainty analysis was calculated using Kline and McClintock method [42]. The uncertainty was calculated using the Eq. (11).

$$U_{\mathrm{R}} = \left[\sum_{\mathrm{i}=1}^{\mathrm{n}} \left(\frac{\partial R}{\partial P_{\mathrm{i}}} \times U_{\mathrm{P_i}}\right)^2\right]^{\frac{1}{2}}, \; 1 \leq \mathrm{i} \leq n, \tag{11}$$

where R and P_{i} are dependent and independent variables, respectively. U_{R} and $U_{\mathrm{P_i}}$ are the uncertainties for the dependent and the independent variables, respectively. The non-dimensional form of Eq. (11) is $((\frac{U_{\mathrm{R}}}{R}) \times 100)$ which is in percentage [42–45]. The independent measured variables used to calculate the experimental uncertainties are summarized in Table 4.

Table 3 Thermal properties of the treated and untreated wood samples. DSC results within parentheses

Thermal properties	BPCM	Untreated woods		Impregnated samples		
		Pine	Beech	Pine/BPCM78%	Pine/BPCM43%	Beech/BPCM38%
Melting point (DSC) ºC	25.5 (24.8)	–	–	25.1 (26.1)	25.4 (26.3)	25.7 (24.9)
Solidifying point (DSC) ºC	21.7; 23.7 (18.5; 22)	–	–	22.7 (21.2; 16.53)	22.7 (18.9; 16)	22.5 (22.2; 17.4)
Melting enthalpy (DSC) J g^{-1}	104 (93)	–	–	44 (42.4)	32 (30.2)	30 (27)
solidifying enthalpy (DSC) J g^{-1}	24; 54 (92.8)	–	–	42 (40.4)	30 (29.1)	30 (26)
Specific heat capacity J g^{-1} K^{-1}	2; 5	2–3	2–3	2.7–4.8	3–4	2.9–3.9
Thermal conductivity W m^{-1} K^{-1}	0.2	0.12	0.23	0.16	0.13	0.255

Table 4 Measured variables, experimental uncertainties and specifications of the used equipment

Measured variable	Nomenclature	Nomenclature of uncertainty	Nominal value	Absolut uncertainty
Heat flux (mean value)	q/a	$U_{\frac{q}{a}}$	64 W m^{-2}	0.001 W m^{-2}
Mean ΔT in heat flow meter	T	U_T	3 °C	0.1 °C
Thickness of the samples	L	U_L	0.009 m	0.00002 m
Maximum $(T_i - T_\infty)_{samp}$ in T-history	T	U_T	23 °C	0.1 °C
Maximum $(T_i - T_\infty)_{ref}$ in T-history	T	U_T	23 °C	0.1 °C
Maximum $(T(t)_n - T_\infty)_{samp}$ in T-history	T	U_T	25 °C	0.1 °C
Maximum $(T(t)_n - T_\infty)_{ref}$ in T-history	T	U_T	25 °C	0.1 °C
Average mass of samples	m	U_m	0.05 kg	0.0000002 kg
Mass of reference	m	U_m	0.66 kg	0.0000002 kg

Thermal conductivity uncertainty calculation

Based on Eqs. 2 and 11, it is possible to calculate the uncertainties of thermal conductivity using the following Eq. 12:

$$U_\lambda = \left[\left(\frac{\partial\lambda}{\partial\frac{q}{a}} \times U_{\frac{q}{a}}\right)^2 + \left(\frac{\partial\lambda}{\partial\Delta L} \times U_L\right)^2 + \left(\frac{\partial\lambda}{\partial\Delta T} \times U_T\right)^2\right]^{1/2} \tag{12}$$

where, $U_{\frac{q}{A}}$, U_L and U_T are, respectively, the uncertainty for heat flux meter, caliper and thermocouple (Table 4). By applying some mathematical calculations, the Eq. 12, evolves into;

$$U_\lambda = \left[\left(\frac{\Delta L}{\Delta T} \times U_{\frac{q}{a}}\right)^2 + \left(\frac{q}{a \times \Delta T} \times U_L\right)^2 + \left(\frac{q \times \Delta L}{a} \times \frac{1}{\Delta T^2} \times U_T\right)^2\right]^{1/2} \tag{13}$$

$$\frac{U_\lambda}{\lambda} = \left[\left(\frac{U_{\frac{q}{a}}}{\frac{q}{a}}\right)^2 + \left(\frac{U_L}{\Delta L}\right)^2 + \left(\frac{U_T}{\Delta T}\right)^2\right]^{1/2} \tag{14}$$

By substituting the nominal and uncertainty values from Table 4, in Eq. 14, the normalized $((\frac{U_R}{R}) \times 100)$ uncertainty associated with the measuring instruments used to determine thermal conductivity was found to be 3.34%.

Enthalpy and C_p uncertainty calculation

Similar approach used for the calculation of the uncertainty associated with thermal conductivity was adopted to calculate the specific heat capacity and enthalpy uncertainties. For this, uncertainty of the heat capacity for reference (Cu) was assumed to be 0 and the nominal value was 0.385 J g^{-1} K^{-1}. Considering Eqs. 9 and 10 together with Eq. 11, the uncertainty for C_p and ΔH are expressed, respectively, as follow:

$$U_{c_p} = \left[\left(\frac{\partial c_p}{\partial m_{ref}} \times U_m\right)^2 + \left(\frac{\partial c_p}{\partial m_{samp}} \times U_m\right)^2 + \left(\frac{\partial c_p}{\partial (T(t)_n - T_\infty)_{ref}} \times U_T\right)^2 + \left(\frac{\partial c_p}{\partial (T(t)_n - T_\infty)_{samp}} \times U_T\right)^2 + \left(\frac{\partial c_p}{\partial (T_i - T_\infty)_{ref}} \times U_T\right)^2 + \left(\frac{\partial c_p}{\partial (T_i - T_\infty)_{samp}} \times U_T\right)^2\right]^{1/2} \tag{15}$$

$$U_{\Delta H} = \left[\left(\frac{\partial \Delta H}{\partial c_{p,samp}} \times U_{c_p}\right)^2 + \left(\frac{\partial \Delta H}{\partial (T(t)_{n,samp} - T_i)} \times U_T\right)^2\right]^{1/2} \tag{16}$$

After mathematical operation, the following Eqs. 17 and 18 are obtained:

$$U_{c_p}=\left[\left(\frac{\ln\left[\frac{(T(t)_n-T_\infty)}{(T_i-T_\infty)}\right]_{ref}}{\ln\left[\frac{(T(t)_n-T_\infty)}{(T_i-T_\infty)}\right]_{samp}}\times\frac{1}{m_{samp}}\times C_{p,ref}\times U_m\right)^2+\left(\frac{\ln\left[\frac{(T(t)_n-T_\infty)}{(T_i-T_\infty)}\right]_{ref}}{\ln\left[\frac{(T(t)_n-T_\infty)}{(T_i-T_\infty)}\right]_{samp}}\times\frac{m_{ref}}{(m_{samp})^2}\times C_{p,ref}\times U_m\right)^2+\left(\frac{\frac{1}{(T(t)_n-T_\infty)_{ref}}}{\ln\left[\frac{(T(t)_n-T_\infty)}{(T_i-T_\infty)}\right]_{samp}}\times\frac{m_{ref}}{m_{samp}}\times C_{p,ref}\times U_T\right)^2+\left(\frac{\ln\left[\frac{(T(t)_n-T_\infty)}{(T_i-T_\infty)}\right]_{ref}}{\left(\ln\left[\frac{(T(t)_n-T_\infty)}{(T_i-T_\infty)}\right]_{samp}\right)^2}\times\frac{(-1)}{(T(t)_n-T_\infty)_{samp}}\times\frac{m_{ref}}{m_{samp}}\times C_{p,ref}\times U_T\right)^2+\left(\frac{\frac{-1}{(T_i-T_\infty)_{ref}}}{\ln\left[\frac{(T(t)_n-T_\infty)}{(T_i-T_\infty)}\right]_{samp}}\times\frac{m_{ref}}{m_{samp}}\times C_{p,ref}\times U_T\right)^2+\left(\frac{\ln\left[\frac{(T(t)_n-T_\infty)}{(T_i-T_\infty)}\right]_{ref}}{\left(\ln\left[\frac{(T(t)_n-T_\infty)}{(T_i-T_\infty)}\right]_{samp}\right)^2}\times\frac{1}{(T_i-T_\infty)_{samp}}\times\frac{m_{ref}}{m_{samp}}\times C_{p,ref}\times U_T\right)^2\right]^{1/2} \quad (17)$$

$$U_{\Delta H}=\left[\left((T(t)_{n,samp}-T_i)\times U_{c_p}\right)^2+\left(c_{p,samp}\times U_T\right)^2\right]^{1/2} \quad (18)$$

The uncertainties for specific heat capacity and enthalpy in non-dimensional form are as:

$$\frac{U_{c_p}}{c_p}=\left[\left(\frac{U_m}{m_{ref}}\right)^2+\left(\frac{U_m}{m_{samp}}\right)^2+\left(\frac{U_T}{(T(t)_n-T_\infty)_{ref}\times\ln\left[\frac{(T(t)_n-T_\infty)}{(T_i-T_\infty)}\right]_{ref}}\right)^2+\left(\frac{-U_T}{(T(t)_n-T_\infty)_{samp}\times\ln\left[\frac{(T(t)_n-T_\infty)}{(T_i-T_\infty)}\right]_{samp}}\right)^2+\left(\frac{-U_T}{(T_i-T(t)_n)_{ref}\times\ln\left[\frac{(T(t)_n-T_\infty)}{(T_i-T_\infty)}\right]_{ref}}\right)^2+\left(\frac{U_T}{(T_i-T_\infty)_{samp}\times\ln\left[\frac{(T(t)_n-T_\infty)}{(T_i-T_\infty)}\right]_{samp}}\right)^2\right]^{1/2} \quad (19)$$

$$\frac{U_{\Delta H}}{\Delta H}=\left[\left(\frac{U_{c_p}}{c_p}\right)^2+\left(\frac{U_T}{(T(t)_{n,samp}-T_i)}\right)^2\right]^{1/2} \quad (20)$$

By replacing the variables in Eq. 17 with the values in Table 4, the heat cavity uncertainty (U_{c_p}) was found to be 0.48 J g^{-1} K^{-1}, which is needed later to calculate uncertainty of enthalpy. The normalized uncertainty ($\left(\frac{U_R}{R}\right)\times 100$) (Eq. 19) associated with the measuring instrument used to calculate heat capacity was found to be 9.6%. The normalized enthalpy uncertainty was then deducted using the calculated U_{c_p}., values in Table 4 and Eq. 20, found to be 9.7%.

Conclusions

Scots pine sapwood and beech wood impregnated with BPCM proved to be composites with enhanced thermal mass with a potential for building applications. The important findings of the study are summarized as follow:

- Wood is a suitable material for "encapsulation" of PCM since it is easy to impregnate at controllable MPG by a combination of vacuum and pressure. Leaching of BPCM is a problem that could not be solved in the present study. Leaching test showed that pine and beech samples leached 8–9% of the impregnated BPCM after 24 h at 35 °C. However, the tested BPCM leached significantly less than PEG 600.
- Rays which are radial anatomical elements in both pine and beech wood served as pathways for impregnation of the BPCM. Part of the tracheid lumens (pine) and vessels (beech) were filled with BPCM which was also found as a precipitate on the cell wall. There is an indication that part of the BPCM can be impregnated in the wood cell wall.
- Thermal conductivity measurement with heat flowmeter method showed that the thermal conductivity of beech is twice as high as that of pine due to its high density. The results showed that, the thermal conductivity of the composites improved after impregnation depending on the MPG of the BPCM.
- DSC results showed that the latent heat of the composites depends on the latent heat of BPCM, by increasing the impregnation retention the latent heat of the composite increases. The phase transition temperatures slightly differed from those of BPCM.
- The thermal mass and heat capacity of the wood/BPCM composites was increased compared with the untreated wood. The untreated wood store/release energy as a sensible heat, while after impregnation the composites can store/release energy in forms of sensible heat before and after phase transition and as a latent heat during the phase transition.

Acknowledgements The study has been carried out within the framework of Smart Energy Systems Research and Innovation Program (ERA-Net E2B2) in the project "Bio-Based Phase Change Materials Integrated into Lignocellulose Matrix for Energy Store in Buildings (BIO-NRG-STORE)". The authors thank also the financial support by

the Swedish Research Council for Sustainable Development (FORMAS), project number 2017-00686.

Funding Open access funding provided by Swedish University of Agricultural Sciences.

Open Access This article is licensed under a Creative Commons Attribution 4.0 International License, which permits use, sharing, adaptation, distribution and reproduction in any medium or format, as long as you give appropriate credit to the original author(s) and the source, provide a link to the Creative Commons licence, and indicate if changes were made. The images or other third party material in this article are included in the article's Creative Commons licence, unless indicated otherwise in a credit line to the material. If material is not included in the article's Creative Commons licence and your intended use is not permitted by statutory regulation or exceeds the permitted use, you will need to obtain permission directly from the copyright holder. To view a copy of this licence, visit http://creativecommons.org/licenses/by/4.0/.

References

1. Ramage MH, Burridge H, Busse-Wicher M, Fereday G, Reynolds T, Shah DU, Wu G, Yu L, Fleming P, Densley-Tingley D, Allwood J. The wood from the trees: the use of timber in construction. Renew Sustain Energy Rev. 2017;68:333–59.
2. Hepburn C, Adlen E, Beddington J, Carter EA, Fuss S, Mac Dowell N, Minx JC, Smith P, Williams CK. The technological and economic prospects for CO 2 utilization and removal. Nature. 2019;575(7781):87–97.
3. Amiri A, Ottelin J, Sorvari J, Junnila S. Cities as carbon sinks—classification of wooden buildings. Environ Res Lett. 2020;15(9):094076.
4. Omer MA, Noguchi T. A conceptual framework for understanding the contribution of building materials in the achievement of sustainable development goals (SDGs). Sustain Cities Soc. 2020;52:101869.
5. Toppinen A, Röhr A, Pätäri S, Lähtinen K, Toivonen R. The future of wooden multistory construction in the forest bioeconomy–a Delphi study from Finland and Sweden. J For Econ. 2018;31:3–10.
6. Wen B, Musa SN, Onn CC, Ramesh S, Liang L, Wang W, Ma K. The role and contribution of green buildings on sustainable development goals. Build Environ. 2020;185:107091.
7. Falk RH. Wood as a sustainable building material. For Prod J. 2009;59(9):6–12.
8. Song S, Leng H, Xu H, Guo R, Zhao Y. Impact of urban morphology and climate on heating energy consumption of buildings in severe cold regions. Int J Environ Res Public Health. 2020;17(22):8354.
9. Nazari M, Jebrane M, Terziev N. Bio-based phase change materials incorporated in lignocellulose matrix for energy storage in buildings—a review. Energies. 2020;13(12):3065.
10. Mathis D, Blanchet P, Landry V, Lagière P. Impregnation of wood with microencapsulated bio-based phase change materials for high thermal mass engineered wood flooring. Appl Sci. 2020;8(12):2696.
11. Khudhair AM, Farid MM. A review on energy conservation in building applications with thermal storage by latent heat using phase change materials. Energy Convers Manage. 2004;45:263–75.
12. De Gracia A, Navarro L, Castell A, Ruiz-Pardo A, Alvárez S, Cabeza LF. Experimental study of a ventilated facade with PCM during winter period. Energy Build. 2013;58:324–32.
13. Chen F, Kessel A, Wolcott M. A novel energy saving wood product with PCM. In: Proceedings of 55th International Convention of Society of Wood Science & Technology, Bejing, China. 2012
14. Li J, Xue P, Ding W, Han J, Guolin S. Micro-encapsulated paraffin/high-density polyethylene/wood flour composite as form-stable phase change material for thermal energy storage. Sol Energy Mater Sol Cells. 2009;93:1761–7.
15. Hu L, Lyu S, Fu F, Huang J, Wang S. Preparation and properties of multifunctional thermochromic energy-storage wood materials. J Mat Sci. 2016;51:2716–26.
16. Hui B, Li Y, Huang Q, Li G, Li J, Cai L, Yu H. Fabrication of smart coatings based on wood substrates with photoresponsive behavior and hydrophobic performance. Mater Des. 2015;84:277–84.
17. Zerriaa A, Ganaoui MEL, Gerardin C, Tazibt A, Gabsi S. Physical incorporation of particles in a porous media: a path to a smart wood. Eur Phys J Appl Phys. 2016. https://doi.org/10.1051/epjap/2015150458.
18. Jiang L, Liu Z, Yuan Y, Wang Y, Lei J, Zhou C. Fabrication and characterization of fatty acid/wood-flour composites as novel form-stable phase change materials for thermal energy storage. Energy Build. 2018;171:88–99.
19. Ma L, Guo C, Ou R, Sun L, Wang Q, Li L. Preparation and characterization of modified porous wood flour/lauric-myristic acid eutectic mixture as a form-stable phase change material. Energy Fuels. 2018;32:5453–61.
20. Guo X, Zhang L, Cao J, Peng Y. Paraffin/wood flour/high-density polyethylene composites for thermal energy storage material in buildings: a morphology, thermal performance, and mechanical property study. Polym Compos. 2018;39:E1643–52.
21. Ma L, Wang Q, Li L. Delignified wood/capric acid-palmitic acid mixture stable-form phase change material for thermal storage. Sol Energy Mater Sol Cells. 2019;194:215–21.
22. Cheng L, Feng J. Form-stable phase change materials based on delignified wood flour for thermal management of buildings. Compos A. 2020;129:105690.
23. Barreneche C, Vecstaudza J, Bajare D, Fernandez AI. PCM/wood composite to store thermal energy in passive building envelopes. IMST IOP Conf Ser Mater Sci Eng. 2017;251:012111.
24. Temiz A, Hekimoglu G, Demirel GK, Sarı A, Amini MHM. Phase change material impregnated wood for passive thermal management of timber buildings. Int J Energy Res. 2020;44(13):10495–505. https://doi.org/10.1002/er.5679.
25. Nazari M, Jebrane M, Terziev N. Multicomponent bio-based fatty acids system as phase change material for low temperature energy storage. J Energy Storage. 2021;39:102645.
26. Adams CWM, Abdulla YH, Bayliss OB. Osmium tetroxide as a histochemical and histological reagent. Histochemie. 1967;9:68–77.
27. Meng X, Gao Y, Wang Y, Yan B, Zhang W, Long E. Feasibility experiment on the simple hot box-heat flow meter method and the optimization based on simulation reproduction. Appl Therm Eng. 2015;83:48–56.
28. Soares N, Martins C, Gonçalves M, Santos P, da Silva LS, Costa JJ. Laboratory and in-situ non-destructive methods to evaluate the thermal transmittance and behavior of walls, windows, and construction elements with innovative materials: a review. Energy Build. 2019;182:88–110.
29. Younsi Z, Joulin A, Zalewski L, Lassue S, Rousse D. Thermophysical characterization of phase change materials with heatflux sensors. In: Proceedings of Eurotherm, 5th European Thermal-Sciences Conference, Eindhoven, The Netherlands. 2008. ISBN 978-90-386-1274-4.

30. Badenhorst H, Cabeza LF. Critical analysis of the T-history method: a fundamental approach. Thermochim Acta. 2017;650:95–105.
31. Solé A, Miró L, Barreneche C, Martorell I, Cabeza LF. Review of the T-history method to determine thermophysical properties of phase change materials (PCM). Renew Sust Energ Rev. 2013;26:425–36.
32. Nazir H, Batool M, Osorio FJB, Ruiz MI, Xu X, Vignarooban K, Phelan P, Kannan AM. Recent developments in phase change materials for energy storage applications: a review. Int J Heat Mass Transf. 2019;129:491–523.
33. Prajapati DG, Kandasubramanian B. Biodegradable polymeric solid framework-based organic phase-change materials for thermal energy storage. Ind Eng Chem Res. 2019;58:10652–77.
34. Liang J, Zhimeng L, Ye Y, Yanjun W, Jingxin L, Changlin Z. Fabrication and characterization of fatty acid/wood-four composites as novel form-stable phase change materials for thermal energy storage. Energy Build. 2018;171:88–99.
35. Jamekhorshid A, Sadrameli SM, Barzin R, Farid MM. Composite of wood-plastic and micro-encapsulated phase change material (MEPCM) used for thermal energy storage. Appl Therm Eng. 2017;112:82–8.
36. Sari A, Alkan C, Karaipekli A, Onal A. Preparation, characterization and thermal properties of styrene maleic anhydride copolymer (SMA)/fatty acid composites as form stable phase change materials. Energy Convers Manage. 2008;49:373–80.
37. Joulin A, Younsi Z, Zalewski L, Lassue S, Rousse DR, Cavrot JP. Experimental and numerical investigation of a phase change material: thermal-energy storage and release. Appl Energy. 2011;88:2454–62.
38. Simpson W, TenWolde A. Physical properties and moisture relations of wood. In: Wood handbook: wood as an engineering material. General technical report FPL-GTR-113. Madison: USDA Forest Service, Forest Products Laboratory; 1999. p. 3.1-3.24.
39. Czajkowski L, Olek W, Weres J. Effects of heat treatment on thermal properties of European beech wood. Eur J Wood Wood Prod. 2020;78:425–31.
40. Yang H, Wang Y, Yu Q, Cao G, Sun X, Yang R, Zhang Q, Liu F, Di X, Li J, Wang C, Li G. Low-cost, three-dimension, high thermal conductivity, carbonized wood-based composite phase change materials for thermal energy storage. Energy. 2018;159:929–36.
41. Yang H, Wang Y, Yu Q, Cao G, Yang R, Ke J, Di X, Liu F, Zhang W, Wang C. Composite phase change materials with good reversible thermochromic ability in delignified wood substrate for thermal energy storage. Appl Energy. 2018;212:455–64.
42. Kline SJ, McClintock F. Describing uncertainties in single-sample experiment. Mech Eng. 1953;75:3–8.
43. Nazari M, Vahid DJ, Saray RK, Mahmoudi Y. Experimental investigation of heat transfer and second law analysis in a pebble bed channel with internal heat generation. Int J Heat Mass Transf. 2017;114:688–702.
44. Moffat RJ. Describing the uncertainties in experimental results. Exp Therm Fluid Sci. 1988;1(1):3–17.
45. Coleman HW, Steele WG. Experimentation, validation, and uncertainty analysis for engineers. 3rd ed. Hoboken: Wiley; 2009.

Publisher's Note Springer Nature remains neutral with regard to jurisdictional claims in published maps and institutional affiliations.